PHILOSOPHICAL TRANSACTIONS A

rsta.royalsocietypublishing.org

Research

Cite this article: Makhnenko RY, Labuz JF. 2016 Elastic and inelastic deformation of fluid-saturated rock. *Phil. Trans. R. Soc. A* **374**: 20150422.
http://dx.doi.org/10.1098/rsta.2015.0422

Accepted: 27 May 2016

One contribution of 12 to a theme issue 'Energy and the subsurface'.

Subject Areas:
civil engineering, geophysics, engineering geology

Keywords:
poroelasticity, drained and undrained response, unjacketed bulk moduli, plane-strain compression, dilatant hardening

Author for correspondence:
Joseph F. Labuz
e-mail: jlabuz@umn.edu

Elastic and inelastic deformation of fluid-saturated rock

Roman Y. Makhnenko[†] and Joseph F. Labuz

Department of Civil, Environmental and Geo- Engineering, University of Minnesota, 500 Pillsbury Drive SE, Minneapolis, MN 55455, USA

JFL, 0000-0002-7549-0644

In situ rock is often saturated with fluid, the presence of which affects both elastic parameters and inelastic deformation processes. Techniques were developed for testing fluid-saturated porous rock under the limiting conditions of drained (long-term), undrained (short-term) and unjacketed (solid matrix) response in hydrostatic, axisymmetric and plane-strain compression. Drained and undrained poroelastic parameters, including bulk modulus, Biot and Skempton coefficients, of Berea sandstone were found to be stress dependent up to 35 MPa mean stress, and approximately constant at higher levels of loading. The unjacketed bulk modulus was measured to be constant for pressure up to 60 MPa, and it appears to be larger than the unjacketed pore bulk modulus. An elasto-plastic constitutive model calibrated with parameters from drained tests provided a first-order approximation of undrained inelastic deformation: dilatant hardening was observed due to pore pressure decrease during inelastic deformation of rock specimens with constant fluid content.

This article is part of the themed issue 'Energy and the subsurface'.

1. Introduction

The presence of pore fluid plays an important role in a wide variety of geophysics and geoengineering problems. These include earthquake precursory processes [1,2], hydraulic fracturing [3–5], water-level changes in wells and tide effects on compressible aquifers [6,7], to name a few. Oil and gas exploration relies

[†]Present address: Laboratory of Soil Mechanics, Chair 'Gaz Naturel' Petrosvibri, Swiss Federal Institute of Technology in Lausanne, EPFL ENAC IIC LMS, GC Station 18, 1015 Lausanne, Switzerland.

THE ROYAL SOCIETY PUBLISHING

on knowledge of the compressibilities and related seismic velocities of rock to differentiate between pore fluids [8,9]. Also, understanding the thermo-hydro-chemo-mechanical interactions between the gas, the groundwater and the host or caprock is critical to evaluate the safety of potential CO_2 storage sites [10].

Two limiting time scales can be considered for the deformation of fluid-filled materials. If the time scale of loading is rapid in comparison with that for diffusion so that the fluid mass in a material element remains constant, then the response is termed undrained. The long-time or drained response is the one for which the local pore fluid pressure is constant. Note that an elastic fluid-saturated solid is stiffer when loading is rapid compared with the time scale of diffusion; e.g. the undrained bulk modulus $K_u \geq K$ the drained modulus [11,12].

The theory of poroelasticity, which describes the elastic response of fluid-filled materials, is attributed to Biot [13,14], who followed the work of Terzaghi [15] on one-dimensional consolidation that accounted for the influence of pore fluid pressure on soil deformation. Biot [14] developed the first rational theory for the three-dimensional mechanical behaviour of isotropic, linearly elastic porous materials. Under the assumption of small strains, linear relationships between stresses, strains, increment of fluid content and pore pressure were written, and four poroelastic moduli, rather than two for standard isotropic elasticity, were introduced [16]. Gassmann [17] derived a relation between the elastic properties of an isotropic porous medium with fluid-filled interconnected pores and the elastic properties of the same medium with empty pores. His work became an important tool in the petroleum industry for interpreting seismic data of sedimentary materials and differentiating between the pore fluids they contain.

Geertsma [18] summarized Biot's and Gassmann's theories and reformulated them in terms of compressibilities, which, as he claimed, were easier to be measured. Geertsma [19] also introduced the term *poroelasticity* with reference to 'Biot's work on the theory of the elasticity and viscoelasticity of fluid-saturated porous solids' and emphasized the similarity between mathematical descriptions of macroscopic poroelasticity and thermoelasticity. Brown & Korringa [20] generalized Gassmann's equation for the case of non-homogeneous material. Their work was used by Rice & Cleary [4], who greatly facilitated the analyses of problems involving interaction between fluid and rock. With no special assumptions regarding the fluid and solid compressibilities, the coupled stress and fluid-flow fields were formulated as an extension of the Biot [14] theory. Detournay & Cheng [5] presented a seminal review of poroelasticity, as well as analytical and numerical methods for solving some fundamental problems, and the various approaches proposed in the literature were unified.

Depending on the stress state, the constitutive response of rock typically involves dilation—incremental volume increase—as deformation becomes inelastic. When the rock is fluid-saturated and the time scale does not allow drainage, suction is induced in the pore fluid, and by the effective stress principle, the rock is dilatantly hardened over the resistance that it would exhibit to a corresponding increment of drained deformation [12]. Further, coupling of deformation with pore fluid diffusion introduces time dependence into the response of an otherwise rate-independent solid. The aim of this study is to investigate poroelastic and inelastic deformation of a porous, fluid-saturated rock under different limiting regimes. The emphasis is placed on accurate force and displacement measurements to determine the parameters that govern material response prior to failure.

2. Theoretical background

(a) Poroelastic relations

The notation and mechanical description of an isotropic poroelastic material from Detournay & Cheng [5] are reviewed. The following is preserved in the expressions presented: ∂ is a partial derivative, d represents an infinitesimal increment and these are used in parameter definitions. Summation by repeating indices is assumed.

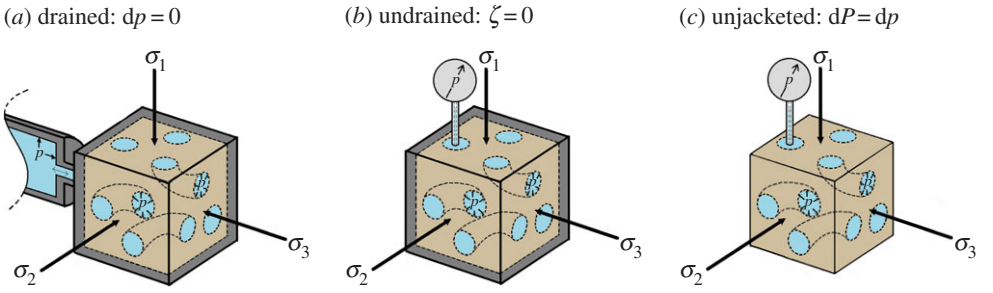

Figure 1. (*a–c*) Sketch of drained, undrained and unjacketed boundary conditions for an element with external principal stresses σ_1, σ_2 and σ_3 and pore pressure p. (Online version in colour.)

The Biot model of a fluid-filled porous material is based on a coherent solid skeleton and a freely moving pore fluid. A material element that occupies volume V in a chosen reference state is considered. On the macroscopic scale of the porous body, this volume element is viewed as an infinitesimal element subjected to locally homogeneous infinitesimal elastic deformation. If the part of V taken by the interconnected pore space is denoted by V_ϕ, the pore volume, then $\phi_o = V_\phi/V$ represents the apparent porosity of the material element in the reference state; $V_s = V - V_\phi$ is the part of V that is taken by the solid skeleton and non-connected pores, if present. The material element is called a representative volume element (RVE) if it consists of a sufficient volume of grains and void space such that a volume average of porosity approaches a stable limit. Each stress and strain variable is defined by its average value over the RVE. The stress state can be represented by the three-dimensional stress tensor σ_{ij} and written in terms of principal stresses $\sigma_1, \sigma_2, \sigma_3$ (figure 1); the mean stress $P = \sigma_{ii}/3 = (\sigma_1 + \sigma_2 + \sigma_3)/3$. The pore pressure p in the element is a scalar and is defined as the pressure in a hypothetical reservoir that is in equilibrium with the element, such that no fluid exchange takes place between the reservoir and the material element. Two strain quantities can be introduced: the small strain tensor ε_{ij} and the variation of fluid content $\zeta = -\mathrm{d}m_f/\rho_f$, where ρ_f is the density of the fluid in the element and $\mathrm{d}m_f$ is the change of its mass over the element volume. Additionally, ζ can be expressed as the variation of fluid volume per unit volume of porous material due to diffusive fluid mass transport:

$$\frac{\partial \zeta}{\partial t} = \frac{\partial q_i}{\partial x_i}, \tag{2.1}$$

where t represents time and q_i is the specific discharge vector, which describes the motion of the fluid relative to the solid in the x_i-direction. The first invariant of ε_{ij} is called volume strain $\varepsilon = \varepsilon_{kk}$. The sign convention of compression positive means that ε_{kk} is positive in compaction and positive ζ corresponds to a loss of fluid by a porous solid.

The stress and the pore pressure are the conjugate quantities of the strain and the variation of the fluid content, respectively. The work increment $\mathrm{d}W$ associated with the strain increments $\mathrm{d}\varepsilon_{ij}$ and $\mathrm{d}\zeta$, in the presence of the stress σ_{ij} and pore pressure p, is

$$\mathrm{d}W = \sigma_{ij}\mathrm{d}\varepsilon_{ij} + p\mathrm{d}\zeta = \varepsilon_{ij}\mathrm{d}\sigma_{ij} + \zeta\,\mathrm{d}p. \tag{2.2}$$

The latter equality is written by assuming reversibility (no energy dissipated during a closed loading cycle) of the deformation process. This assumption was used by Biot [14], along with linearity between the stress (σ_{ij}, p) and the strain (ε_{ij}, ζ), to write the constitutive relations by extending the known elastic expressions. Biot's constitutive constants, which characterize the coupling between the solid and fluid stress and strain, cannot be directly measured in laboratory experiments, so they are not presented here. Instead, the response of a fluid-saturated porous material is described in terms of two limiting behaviours, drained and undrained, the definitions of which follow.

The drained condition corresponds to the case of constant pore pressure: $\mathrm{d}p = 0$. This condition can be achieved by connecting a specimen to a large reservoir with constant fluid pressure p (figure 1*a*). For simplification, the constitutive equations related to the drained material behaviour are written only for the case of zero pore pressure $p = 0$. Drained bulk modulus K can be expressed in terms of changes of the external mean stress with volume strain: $K = V(\mathrm{d}P/\mathrm{d}V)|_{\mathrm{d}p=0}$. If the case of zero pore pressure is assumed, then from the linearity of the stress–strain relationships, the volume strain and the variation in the fluid content can be written as

$$\varepsilon = \frac{P}{K} \tag{2.3}$$

and

$$\zeta = \alpha\varepsilon, \tag{2.4}$$

where the constant α is the ratio of the fluid volume gained or lost in a material element due to loading, to the volume change of that element, when the pore pressure is preserved constant. As the change of fluid volume in the element cannot be greater than the total volume change, and both of them should have the same sign, $0 \le \alpha \le 1$. Note that α is exactly one if all of the volume strain is due to pore volume change equal to the change of fluid volume. It means that the solid phase can be considered incompressible, which is the case for soft soil, but not for rock, where the pore volume change is comparable with the change of solid volume.

The undrained response characterizes the condition where the fluid is trapped in the porous solid such that $\zeta = 0$. The undrained test can be represented by the specimen, subjected to mean stress P, with a casing or jacket around it, which does not allow fluid escaping or entering the specimen but does allow the measurement of pore pressure (figure 1*b*). Undrained bulk modulus K_{u} can be defined as $K_{\mathrm{u}} = V(\mathrm{d}P/\mathrm{d}V)|_{\zeta=0}$. Because ζ is assumed to be a linear function of P and p, the following relationship holds for the undrained case ($\zeta = 0$):

$$p = BP, \tag{2.5}$$

where B is the Skempton [21] coefficient ($0 \le B \le 1$). The undrained volumetric response can be written as

$$\varepsilon = \frac{P}{K_{\mathrm{u}}}. \tag{2.6}$$

The bulk modulus of the pore fluid K_{f} can also be defined as $K_{\mathrm{f}} = V_{\mathrm{f}}\ (\mathrm{d}p/\mathrm{d}V_{\mathrm{f}})$, where V_{f} is the volume of the fluid.

For the drained condition, the increase in load is taken by the rock skeleton only. So the specimen deforms more than for loading applied under the undrained condition, where the pore fluid takes part of the load and also compresses, hence $0 \le K \le K_{\mathrm{u}}$. Generally, the drained and undrained conditions are the limiting cases of slow and fast loading, respectively. Little fluid exits or enters the RVE if the loading is rapid, hence $\zeta = 0$ under the undrained condition. When the fluid flow has enough time to equilibrate with the external boundary, the fluid pressure is constant in the RVE, $\mathrm{d}p = 0$, which is the characteristic of the drained response.

The constitutive equations of an isotropic poroelastic material conveniently are separated into deviatoric strain $e_{ij} = \varepsilon_{ij} - \varepsilon\delta_{ij}/3$ and volumetric strain ε; δ_{ij} is the Kronecker delta. The deviatoric strain can be expressed through deviatoric stress ($\sigma_{ij} - P\delta_{ij}$):

$$e_{ij} = \frac{1}{2G}(\sigma_{ij} - P\delta_{ij}), \tag{2.7}$$

where G is shear modulus. The volumetric strain is written based on the linearity of the stress–strain relations and equations (2.3)–(2.6):

$$\varepsilon = \frac{1}{K}(P - \alpha p) \tag{2.8}$$

and

$$\zeta = \frac{\alpha}{K}\left(P - \frac{p}{B}\right). \tag{2.9}$$

The volumetric relations can be written inversely as

$$P = K_u \varepsilon - M\alpha\zeta \tag{2.10}$$

and

$$p = M(\alpha\varepsilon - \zeta), \tag{2.11}$$

where M is the inverse of the increase of the fluid content caused by the increase of the pore pressure and is sometimes called the Biot modulus, $M = (\mathrm{d}p/\mathrm{d}\zeta)|_{\mathrm{d}\varepsilon=0} = (K_u - K)/\alpha^2$.

The presented constitutive model describes the response of the material as a whole, without taking into account the individual contributions of its solid and fluid constituents. These contributions can be considered if a micromechanical approach is used. For the needs of this work, it is convenient to introduce the so-called unjacketed condition. The unjacketed test was proposed by Biot & Willis [16] and it is characterized by equal increments in mean stress and pore pressure, $\mathrm{d}P = \mathrm{d}p$ (figure 1*c*): the specimen with no jacket or membrane is loaded by a fluid that is allowed to penetrate inside the specimen and thus equilibrate the mean stress with the pore pressure. The test can also be carried out on a jacketed specimen by imposing equal increments of pore pressure and mean stress, without the requirement of the equality of P and p. Rice & Cleary [4] introduced two other material constants: unjacketed bulk modulus $K_s' = V(\mathrm{d}P/\mathrm{d}V)|_{\mathrm{dP=dp}}$ and unjacketed pore volume bulk modulus $K_s'' = V_\phi(\mathrm{d}P/\mathrm{d}V_\phi)|_{\mathrm{dP=dp}}$.

Generally, the coefficients K_s' and K_s'' are different; K_s' is related to the total volume change in unjacketed loading, while K_s'' is associated with the change only in the pore volume V_ϕ. However, under certain conditions, they both can be identified with the bulk modulus of the solid constituent $K_s = V_s(\mathrm{d}P/\mathrm{d}V_s)|_{\mathrm{dP=dp}}$. Assuming that the rock has fully connected pore space, all points of the solid phase may be taken as elastically isotropic with the same local bulk modulus K_s, and as both fluid and solid are chemically inert for the time scale of the tests, it can be shown that $K_s = K_s' = K_s''$ [4]. However, this assumption may not be valid for sedimentary rock, where intergranular cement and pore lining have different elastic properties [22,23]. A difference between K_s' and K_s'' can also be a consequence of non-connected pore space [5].

If the constitutive response (2.8) is considered under the unjacketed condition ($P = p$), it can be shown that α, referred to as the Biot coefficient [24], is

$$\alpha = 1 - \frac{K}{K_s'}. \tag{2.12}$$

The relationship between drained and undrained bulk moduli is called the generalized Gassmann equation [20] and can be written as

$$K_u = K + \frac{\alpha^2 K}{(1-\alpha)\alpha + \phi_o K(1/K_f - 1/K_s'')}. \tag{2.13}$$

Equations (2.8), (2.9) and (2.13) provide a general expression for the Skempton coefficient B:

$$B = \frac{K_u - K}{\alpha K_u} = \frac{\alpha}{\alpha + \phi_o K(1/K_f - 1/K_s'')}. \tag{2.14}$$

From equations (2.12) and (2.14) and the range of α and B, the following inequality can be written:

$$0 \le K \le K_u \le K_s'. \tag{2.15}$$

The emphasis on the volumetric response reflected the choice of bulk moduli K and K_u as a part of fundamental set of material constants. Alternatively, drained and undrained Poisson's ratios, ν and ν_u, can be chosen for the presentation of the linear theory. They are related to K, K_u and G

according to

$$\left.\begin{aligned} \nu &= \frac{3K - 2G}{2(3K + G)} \\ \text{and} \quad \nu_{\mathrm{u}} &= \frac{3K_{\mathrm{u}} - 2G}{2(3K_{\mathrm{u}} + G)}. \end{aligned}\right\} \tag{2.16}$$

From inequality (2.15), it follows $0 \le \nu \le \nu_{\mathrm{u}} \le 0.5$, where $\nu_{\mathrm{u}} = 0.5$ and $\alpha = 1$ holds for the case of incompressible constituents, which is characterized by the strongest poroelastic effect, a reasonable approximation for soft soil. Note that in the case of $\nu_{\mathrm{u}} \cong \nu$, the effect of undrained loading disappears.

The Skempton pore pressure coefficient B and the Biot modulus M can also be expressed in terms of ν and ν_{u}:

$$\left.\begin{aligned} B &= \frac{3(\nu_{\mathrm{u}} - \nu)}{\alpha(1 - 2\nu)(1 + \nu_{\mathrm{u}})} \\ \text{and} \quad M &= \frac{2G(\nu_{\mathrm{u}} - \nu)}{\alpha^2(1 - 2\nu_{\mathrm{u}})(1 - 2\nu)}. \end{aligned}\right\} \tag{2.17}$$

The constitutive equations (2.8)–(2.11) can be written with G, α, ν and ν_{u}, and (2.8) is

$$2G\varepsilon_{ij} = \sigma_{ij} - \frac{\nu}{1 + \nu}\sigma_{kk}\delta_{ij} - \frac{\alpha(1 - 2\nu)}{1 + \nu}p\delta_{ij}, \tag{2.18}$$

and it can be also presented as

$$\sigma_{ij} - \alpha p\delta_{ij} = 2G\varepsilon_{ij} + \frac{2G\nu}{1 - 2\nu}\varepsilon\delta_{ij}. \tag{2.19}$$

These relations are similar to those for a drained elastic solid with $(\sigma_{ij} - \alpha p\delta_{ij})$ playing the role of an 'effective stress', so α is sometimes called the effective stress coefficient [24]. For the case of $p = 0$, (2.18) and (2.19) reduce to the drained (or dry) constitutive relation.

If ζ is taken as the coupling term, then the constitutive expressions become

$$2G\left(\varepsilon_{ij} - \frac{B}{3}\zeta\delta_{ij}\right) = \sigma_{ij} - \frac{\nu_{\mathrm{u}}}{1 + \nu_{\mathrm{u}}}\sigma_{kk}\delta_{ij} \tag{2.20}$$

and

$$\sigma_{ij} = 2G\varepsilon_{ij} + \frac{2G\nu_{\mathrm{u}}}{1 - 2\nu_{\mathrm{u}}}\varepsilon\delta_{ij} - \alpha M\zeta\delta_{ij}. \tag{2.21}$$

Equations (2.18)–(2.21) clearly show the elastic character of the poroelastic material in its two limiting behaviours, drained ($p = 0$) and undrained ($\zeta = 0$).

(b) Inelastic response

The constitutive model chosen for describing the inelastic response of fluid-saturated rock was formulated by Rice [12] for the plane-strain deformation state of confined shearing. It illustrates the hardening effect of dilatancy-induced pore pressure reduction. The model was reformulated by Rudnicki [25] in terms of poroelastic parameters for rock subjected to pore pressure p, shear stress τ and constant mean stress P. The model extended for the case of $\mathrm{d}P \neq 0$ is presented here.

For stress increments $\mathrm{d}\tau, \mathrm{d}(P - p)$ that involve continued inelastic deformation, the increments of shear strain $\mathrm{d}\gamma$ and volume strain $\mathrm{d}\varepsilon$ (compression positive) are

$$\mathrm{d}\gamma = \frac{\mathrm{d}\tau}{G} + \mathrm{d}\gamma^{\mathrm{p}} \tag{2.22}$$

and

$$\mathrm{d}\varepsilon = \frac{\mathrm{d}P}{K} + \mathrm{d}\varepsilon^{\mathrm{p}}, \tag{2.23}$$

where $\mathrm{d}\gamma^{\mathrm{p}}$ and $\mathrm{d}\varepsilon^{\mathrm{p}}$ are the increments of inelastic shear and volume strain, respectively. An increase in mean stress inhibits inelastic deformation in brittle rock. Thus, the inelastic increment

of shear strain takes the form

$$\mathrm{d}\gamma^{\mathrm{p}} = \frac{\mathrm{d}\tau - \mu \mathrm{d}P}{H}, \tag{2.24}$$

where H is an inelastic hardening modulus and μ is a friction parameter, which can be measured as the local slope of the yield surface separating elastic and inelastic states in the plane of τ and $P - p$. For the drained response ($\mathrm{d}p = 0$), $\mathrm{d}\tau$ can be written as

$$\mathrm{d}\tau = \frac{H}{1 + H/G}\mathrm{d}\gamma + \frac{\mu}{1 + H/G}\mathrm{d}P. \tag{2.25}$$

The inelastic volume strain, negative for dilating rock, arises from processes that accompany inelastic shear and its increment is given by β, the dilatancy factor ($\beta < 0$ for compaction):

$$\mathrm{d}\varepsilon^{\mathrm{p}} = -\beta \cdot \mathrm{d}\gamma^{\mathrm{p}}. \tag{2.26}$$

To include the effects of pore fluid pressure, the total mean stress is replaced by the effective mean stress. For elastic deformation, the effective mean stress is written in Biot's form: $P - \alpha p$ (equation (2.8)). For inelastic deformation arising from opening and sliding of microcracks with small contact areas, Rice [26] has shown that the appropriate form of the effective mean stress is the Terzaghi effective pressure $P' = P - p$. This deduction is consistent with experimental observations on inelastic properties of brittle rock [11]. Thus, the increments of shear and volume strain are

$$\mathrm{d}\gamma = \frac{\mathrm{d}\tau}{G} + \frac{[\mathrm{d}\tau - \mu(\mathrm{d}P - \mathrm{d}p)]}{H} \tag{2.27}$$

and

$$\mathrm{d}\varepsilon = \frac{\mathrm{d}P - \alpha \mathrm{d}p}{K} - \frac{\beta[\mathrm{d}\tau - \mu(\mathrm{d}P - \mathrm{d}p)]}{H}. \tag{2.28}$$

The inelastic variation in the fluid content ζ^{p} was shown to be the plastic dilatancy: $\zeta^{\mathrm{p}} = \mathrm{d}\varepsilon^{\mathrm{p}}$ [26]. The total ζ is the sum of its elastic and inelastic increments; hence equations (2.9) and (2.14) are extended for the case of current porosity (ϕ instead of ϕ_{o}):

$$\zeta = \frac{\alpha(\mathrm{d}P - \mathrm{d}p)}{K} - \phi \mathrm{d}p\left(\frac{1}{K_{\mathrm{f}}} - \frac{1}{K_{\mathrm{s}}''}\right) + \mathrm{d}\varepsilon^{\mathrm{p}}. \tag{2.29}$$

For undrained response, $\zeta = 0$ in (2.29) and considering (2.28) yields

$$\mathrm{d}p = \frac{-\beta K_{\mathrm{eff}}}{H + \mu\beta K_{\mathrm{eff}}}\mathrm{d}\tau + \frac{\alpha K_{\mathrm{eff}} H/K + \mu\beta K_{\mathrm{eff}}}{H + \mu\beta K_{\mathrm{eff}}}\mathrm{d}P, \tag{2.30}$$

where K_{eff} can be written as

$$\frac{1}{K_{\mathrm{eff}}} = \phi\left(\frac{1}{K_{\mathrm{f}}} - \frac{1}{K_{\mathrm{s}}''}\right) + \frac{\alpha}{K}. \tag{2.31}$$

Therefore, for dilatant inelastic deformation ($\beta > 0$), the pore fluid pressure tends to decrease. When (2.30) is substituted into (2.27), the result is

$$\mathrm{d}\tau = \frac{(H + \mu\beta K_{\mathrm{eff}})}{1 + (H + \mu\beta K_{\mathrm{eff}})/G}\mathrm{d}\gamma + \frac{\mu(1 - \alpha K_{\mathrm{eff}}/K)}{1 + (H + \mu\beta K_{\mathrm{eff}})/G}\mathrm{d}P. \tag{2.32}$$

If $\mathrm{d}P = 0$ in (2.25), (2.30) and (2.32), then the presented model is the same as Rudnicki [25], and because the hardening modulus has been augmented by the term $\mu\beta K_{\mathrm{eff}}$ in (2.32) compared with the drained case (2.25), the response is stiffer and the rock is said to be dilatantly hardened. If the mean stress is changing during the deformation, then the hardening effect is not clearly pronounced and is dependent on the value of $(1 - \alpha K_{\mathrm{eff}}/K)$. The parameter $K_{\mathrm{eff}} = K_{\mathrm{eff}}(P')$ is stress dependent, and its development with Terzaghi effective mean stress is evaluated, and along with the other material constants, used to determine undrained response.

3. Experimental methods

(a) Hydrostatic compression

One of the simplest tests for measurements of the bulk material properties is hydrostatic compression. Specimens instrumented with sets of strain rosettes can be placed inside a pressure chamber and subjected to mean stress P (figure 2*a*). Volume strain ε can be calculated as the trace of the three-dimensional strain tensor ε_{ij} (the first invariant), and hence the measurements of the strains in any three perpendicular directions x, y, z are enough for determining $\varepsilon = \varepsilon_{xx} + \varepsilon_{yy} + \varepsilon_{zz} = \varepsilon_{d_1} + \varepsilon_{d_2} + \varepsilon_{d_3}$.

Jacketed and unjacketed hydrostatic compression tests are performed on prismatic rock specimens instrumented with sets of strain rosettes. Dry sandstone specimens covered with polyurethane are placed inside a pressure chamber and loaded to 60 MPa. Measured jacketed bulk modulus K can be considered as the drained bulk modulus of the material for the special case of zero pore pressure ($p = 0$). After that, the jacket is removed and the confining fluid is allowed to penetrate into the rock. Hydraulic oil is used as the confining fluid because it has no electrical effect on strain gauge connections and no chemical effect on the tested rock in the short term. After at least 24 h of saturation at 20–30 MPa pore pressure, unjacketed loading ($P = p$ and $\Delta P = \Delta p$) up to 60 MPa and unloading are performed. Here Δ designates increments of quantities that are measured experimentally. The unjacketed bulk modulus is then calculated from measurements of volume strain.

(b) Plane-strain and axisymmetric compression

Drained and undrained compression experiments are conducted with a Vardoulakis–Goldscheider type of plane-strain apparatus [27,28] specifically modified and calibrated for testing fluid-saturated rock [29]. Prismatic specimens, $100 \times 87 \times 44$ mm, are covered with polyurethane and wedged inside the stiff frame in a way that the stress in the plane-strain direction is higher than the desired cell pressure. Generally, the frame restricts ε_2 (it is two orders of magnitude smaller than ε_1) and thus applies the intermediate principal stress σ_2. Deformation of the frame is measured by strain gauges and can be related to the deformation of the specimen in that direction. Major principal stress σ_1 is applied in the vertical (axial) direction and is called axial stress, minor principal stress σ_3 is applied laterally by the confining fluid and is called cell pressure (figure 2*b*). Lateral and axial deformations are accurately measured by sets of linear variable differential transformers (LVDTs) and allow the calculation of strains ε_1 and ε_3 aligned with the major and minor principal stresses. The intermediate principal stress cannot be controlled, but it can be calculated from generalized Hooke's law for an isotropic linearly elastic solid:

$$\sigma_2 = E\varepsilon_2 + \nu(\sigma_1 + \sigma_3). \tag{3.1}$$

Based on wave velocity measurements up to peak stress, the elastic parameters in the plane-strain direction are not affected appreciably [29].

Performing a test at constant confining pressure ($\Delta\sigma_3 = 0$) and taking the sign convention of compression positive, Young's modulus E and Poisson's ratio ν are

$$\left.\begin{aligned} E &= \Delta\sigma_1 \frac{\Delta\varepsilon_1 - 2\Delta\varepsilon_3}{(\Delta\varepsilon_1 - \Delta\varepsilon_3)^2} \\ \text{and} \qquad \nu &= \frac{-\Delta\varepsilon_3}{\Delta\varepsilon_1 - \Delta\varepsilon_3}. \end{aligned}\right\} \tag{3.2}$$

For plane problems, it is convenient to introduce the invariants named (i) average stress $s = (\sigma_1 + \sigma_3)/2$, (ii) shear stress $t = (\sigma_1 - \sigma_3)/2$, (iii) volume strain $\varepsilon = (\varepsilon_1 + \varepsilon_3)/2$, and (iv) shear strain $\gamma = (\varepsilon_1 - \varepsilon_3)/2$. This set of invariants satisfies the requirement of preserving the work increment $\mathrm{d}W$

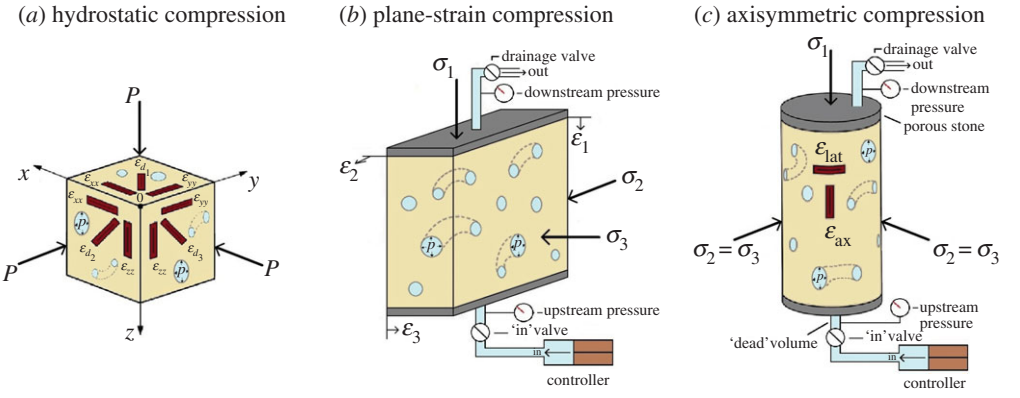

Figure 2. (*a–c*) Experimental configurations for the hydrostatic, plane-strain and axisymmetric (triaxial) compression tests with applied principal stresses, pore pressure and corresponding strains. (Online version in colour.)

constant while changing the coordinate system:

$$dW = \sigma_1 d\varepsilon_1 + \sigma_2 d\varepsilon_2 + \sigma_3 d\varepsilon_3 = s d\varepsilon + t d\gamma. \tag{3.3}$$

Generalized Hooke's law for plane strain becomes

$$\left.\begin{aligned} \Delta\varepsilon &= \frac{2(1+\nu)}{3K}\Delta s \\ \text{and} \quad \Delta\gamma &= \frac{1}{G}\Delta t. \end{aligned}\right\} \tag{3.4}$$

Hence drained and undrained bulk moduli K and K_u and shear modulus G can be determined. Because change in pore pressure does not affect the shear stress, drained and undrained shear moduli for isotropic rock are equal. Measurements of K then allow the calculation of the unjacketed bulk modulus K'_s.

A drained test can be performed by maintaining the pore pressure in the specimen constant; this condition is applied and preserved by connecting the pore-water lines to a microprocessor-based hydraulic pump that maintains water pressure at a constant value, within a tolerance of 0.01 MPa. By closing the inlet and drainage valves (figure 2*b*) and thus keeping the mass of the fluid in the specimen constant, the undrained testing condition can be achieved. Once ν, E, ν_u and E_u are obtained from drained and undrained plane-strain tests, other parameters such as K, K_u and G can be calculated. Another parameter that can be measured under the undrained condition is the Skempton coefficient B. The detailed description of the saturation process and measurement of B is given in §3e.

Another geometry that allows direct measurements of applied principal stresses and corresponding strains is a cylindrical specimen tested in conventional triaxial (axisymmetric) compression (figure 2*c*). The plane-strain apparatus was modified to allow testing of a cylindrical specimen ($H = 104.0$ mm, $D = 50.8$ mm), in the chamber filled with hydraulic oil. In conventional triaxial compression, the major principal stress $\sigma_1 = \sigma_{axial}$ is applied axially while the intermediate and minimum principal stresses are applied in the radial direction by the confining fluid; thus $\sigma_2 = \sigma_3 = \sigma_{radial}$ and σ_3 is called the cell pressure. Axial strain ε_1 is measured by strain gauges $\varepsilon_1 = \varepsilon_{axial}$ and LVDTs; tangential and radial strains ε_θ and ε_r are equal to each other and are measured by lateral strain gauges: $\varepsilon_\theta = \varepsilon_r = \varepsilon_2 = \varepsilon_3 = \varepsilon_{lateral}$ (figure 2*c*). For this geometry, mean stress $P = (\sigma_1 + 2\sigma_3)/3$ and volume strain $\varepsilon = \varepsilon_1 + 2\varepsilon_3$.

Because application and measurement of the three principal stresses and corresponding strains are straightforward in conventional triaxial compression, unjacketed test can be conducted by applying increments of pore pressure equal to the increments in the mean stress: $\Delta p = \Delta P$.

Drained and undrained compression are performed by preserving the same boundary conditions as in plane-strain compression. The bulk moduli related to these three limiting states, i.e. unjacketed K'_s, drained K and undrained K_u, can be measured by applying hydrostatic loading to the cylindrical specimens and recording the corresponding volume strain and provide the calculation of the other poroelastic parameters from equations (2.12)–(2.14). If axial and cell pressures are applied separately, drained and undrained Young's moduli and Poisson's ratios can also be measured.

Moreover, performing plane-strain or axisymmetric loading under drained conditions and assuming full saturation of the rock, such that the volume of the fluid in the pores is equal to the pore volume of the specimen, the volume of the fluid drained away from it during elastic deformation can be precisely measured. Following the definition of α (equation (2.4)), it is possible to calculate α as the ratio between the drained fluid volume ΔV_f and the change in specimen volume ΔV [5]:

$$\alpha = \frac{\Delta V_f}{\Delta V}. \tag{3.5}$$

Additionally, K''_s can be measured by performing an unjacketed test ($dP = dp$) under axisymmetric conditions. Following the suggestion by Cheng [30] and accounting for the compressibility of pore pressure tubing and controller C_{L+M}, fluid volume expelled or injected in the rock due to loading or unloading can be written as

$$\frac{-\Delta V_f}{\Delta p} = (V_L + V_m)\, C_{L+M} + \frac{V_L + V_m + \phi V}{K_f} - \frac{\phi V}{K''_s}, \tag{3.6}$$

where V_L and V_m are the fluid volumes in the pore water lines and pore pressure controller, respectively. These parameters are discussed in §3c. Directly measured K''_s has not been widely reported.

(c) Drainage system

In plane-strain and axisymmetric compression experiments with fluid-saturated rock, the specimen is connected to the drainage system of the cell and also to pore pressure transducers (figure 2*b*,*c*). As the drainage system has a non-zero volume filled with water, it experiences volume changes due to its compressibility if pore pressure is changing, which is the case of an undrained test. The variations of the volume of the drainage system and of the fluid content induce fluid flow into or out of the specimen to achieve pressure equilibrium between the specimen and the drainage system. This fluid mass exchange modifies measured pore pressure and hence measured strains. Wissa [31] and Bishop [32] modified the expression for the Skempton coefficient B to include terms representing the compressibility of the pore pressure system:

$$B = \frac{1}{[(\Delta p/\Delta P)^{\text{measured}}]^{-1} - (V_L/V)K/\alpha K_f - K(C_L + C_M)/\alpha V}, \tag{3.7}$$

where V_L is the volume of the fluid in the pore-water lines, C_L is the compressibility of the pore-water lines and C_M is the compressibility of the pore pressure measuring element. Note that C_{L+M} from equation (3.6) is larger than $C_L + C_M$, because in the former case the pore pressure controller serves as the pressure measuring element instead of the pressure transducer in the latter case. Several researchers [32–34] noted that for modern high-pressure stainless steel tubing and pressure transducers, the main contribution (more than 95%) to the correction term comes from the extra fluid volume in the system V_L, which is confirmed by calibration tests showing that the third term in the denominator of the right-hand side of (3.7) is less than 0.01. Consequently, only the first two terms are considered and V_L is measured to be 14 ml for the plane-strain configuration (typical specimen volume $V = 380$ ml) and 12 ml in axisymmetric compression ($V = 210$ ml). Ghabezloo & Sulem [34] also introduced extra correction terms due to the effect of temperature on the drainage system and pore fluid density, but these are not considered in our case, as all tests were performed at constant room temperature (24°C). The corrected expression

for undrained bulk modulus, which can be derived by combining equations (2.14) and (3.7) is obtained [34]:

$$K_{\mathrm{u}} = K\left(1 - \left[\left(1 - \frac{K}{K_{\mathrm{u}}^{\mathrm{measured}}}\right)^{-1} - \frac{V_L}{V}\frac{K}{\alpha^2 K_{\mathrm{f}}}\right]^{-1}\right)^{-1}. \tag{3.8}$$

Analogously, expressions for corrected undrained Poisson's ratio and Young's modulus can be written using equations (2.17) and relationships between elastic constants:

$$\nu_{\mathrm{u}} = \nu + \left(\frac{1}{\nu_{\mathrm{u}}^{\mathrm{measured}} - \nu} - \frac{V_L}{V}\frac{3K}{\alpha^2 K_{\mathrm{f}}(1-2\nu)(1+\nu)}\right)^{-1} \tag{3.9}$$

and

$$E_{\mathrm{u}} = 3\left[\left(1 - \left[\left(1 + \frac{3K}{G} - \frac{9K}{E_{\mathrm{u}}^{\mathrm{measured}}}\right)^{-1} - \frac{V_L}{V}\frac{K}{\alpha^2 K_{\mathrm{f}}}\right]^{-1}\right)\Big/ 3K + \frac{1}{G}\right]^{-1}. \tag{3.10}$$

(d) Berea sandstone

Berea sandstone is a fine-grained (0.12–0.25 mm), well-compacted, cross-bedded sandstone with a dominant pore diameter of 20 μm. It mainly consists of sub-rounded to rounded quartz grains, approximately 90% of solid volume, K-feldspar (approx. 7%), calcite (approx. 1%), iron oxide (approx. 0.5%) and traces of other minerals. Cementation of the sandstone occurs mainly as interstitial microquartz and syntaxial quartz overgrowths. The rock is light grey with closely spaced (approx. 5 mm) planar bedding surfaces clearly demarked by laminations of rust-red iron oxides. The material has interconnected porosity $\phi_{\mathrm{o}} = 0.23$ and intrinsic permeability $k = 4 \times 10^{-14}\,\mathrm{m}^2$ (measured perpendicular to the beds at $P' = 5$ MPa), which allows studying deformation of fluid-saturated porous rock at reasonable time scales. A single block, 305 × 305 × 245 mm with density $\rho = 2060\,\mathrm{kg\,m^{-3}}$ was used to fabricate all specimens. Uniaxial compressive strength (UCS) tests were performed on six right cylindrical specimens, height $H = 105$ mm and diameter $D = 50$ mm, prepared in accordance with ISRM standards [35] and loaded at an axial displacement rate of $5 \times 10^{-4}\,\mathrm{mm\,s^{-1}}$. Axial and tangential strains were monitored by foil strain gauges attached to one side of a specimen to determine E and ν. An opposite side was ground and painted so that the digital image correlation (DIC) technique could be used for calculation of the displacement field [36]. The UCS measured in the direction perpendicular to the bedding planes was found to be 41–43 MPa, which is 7–8% larger than the one along the beds. Young's modulus and Poisson's ratio measured by strain gauges and calculated by the DIC method were found to be consistent, with $E = 11$–13 GPa and $\nu = 0.31$.

The characteristic time for dissipation of the induced pore pressure in a specimen with a characteristic length L drained at two ends is of order $L^2/4c$, where c is the diffusivity coefficient [5], which can be expressed by the permeability k, fluid viscosity μ and poroelastic parameters:

$$c = \frac{2kG(1-\nu)(\nu_{\mathrm{u}} - \nu)}{\mu\alpha^2(1-2\nu)^2(1-\nu_{\mathrm{u}})}. \tag{3.11}$$

Values of c for water-saturated Berea sandstone are of the order of $0.1\,\mathrm{m^2\,s^{-1}}$. The characteristic time scale for equilibration of pore pressure inside the rock is approximately 0.1 s for water-filled sandstone and approximately 10 s for oil-filled sandstone, which is significantly smaller than the time scales of the reported tests (1000 s or more).

(e) Saturation

Even a small variation in the degree of saturation strongly influences the bulk modulus of the fluid and hence K_{u} and B as indicated by equations (2.13) and (2.14). The back pressure saturation technique, described in [37], was implemented: after applying desired mean stress and flushing deaired water through the rock until the steady-state flow was achieved and a few pore volumes of water go through the specimen, increments of pore (or back) pressure were applied while

keeping the Terzaghi effective pressure $P' = P - p$ approximately the same. The purpose of the back pressure technique is to achieve 100% saturation by forcing any gas into solution of the pore water. Increase of the pore pressure in a partially saturated specimen affects the volume of the gas in the pores in two ways: (i) by direct compression, the gas is reduced in volume according to Boyle's law; (ii) by application of a higher pressure, additional amounts of gas are dissolved in the pore water in accordance with Henry's law of solubility [38]. Wissa [31] suggested a method to check if a very stiff soil specimen is fully saturated by determining Skempton's B coefficient at gradually increasing back pressures while keeping the Terzaghi effective mean stress constant. If the rock is not fully saturated, then the B-value will be increasing with increasing pressure, as more air is forced into solution. A measured B-value that is constant and independent of the magnitude of the back pressure indicates full saturation. Once the air is driven into solution, the air–water mixture behaves as a fluid with a bulk modulus equal to that of pure water [39], so dissolved air in the water has no influence on K_f. Hence, pore fluid bulk modulus becomes a fixed parameter and can be used in calculation of some other poroelastic moduli. In the case of a specimen fully saturated with water, $K_f = K_{water} = 2.24\,\text{GPa}$.

Calculation of the Skempton coefficient B is not straightforward under a plane-strain condition, because the intermediate principal stress is not measured directly, but calculated with the knowledge of elastic parameters (equation (3.1)). The specimen size was chosen so that when equal increments in axial stress $\Delta\sigma_1$ and cell pressure $\Delta\sigma_3$ were applied, the frame deformation due to the stress increment applied by the specimen was compensated by the negative strain on the inner side of the frame due to the increase in cell pressure; according to Lame's solution, the inner part compresses due to equal pressure applied on the inside and outside of the cylinder. So, $\Delta\varepsilon_2 = 0$ in equation (3.1) and the expression for the measured B takes the form

$$B^{\text{measured}} = \left(\frac{\Delta p}{\Delta P}\right)^{\text{measured}} = \frac{3\Delta p}{(1+\tilde{\nu})(\Delta\sigma_1 + \Delta\sigma_3)}, \tag{3.12}$$

where $\tilde{\nu}$ is the current Poisson's ratio of the rock and it changes from ν in dry (or drained) condition to ν_u upon saturation, while $\nu_u > \nu$. When the undrained elastic loading is performed on the saturated specimen, ν_u independent of B-values can be calculated from the plane-strain compression data. The pore pressure increment will increase with growing back pressure because the degree of saturation is augmented and consequently the bulk modulus of the pore fluid increases as the back pressure is growing [31]. When Δp becomes the same for each increment $\Delta\sigma_1 = \Delta\sigma_3 = \text{const.}$, the rock is considered to be saturated. Measurement of B is direct for cylindrical specimens tested in conventional triaxial compression: as hydrostatic pressure is applied, $\Delta P = \Delta\sigma_1 = \Delta\sigma_2 = \Delta\sigma_3$.

The B-values (equation (3.7)) for axisymmetric compression tests conducted at $P' = 5\,\text{MPa}$ are presented in figure 3, along with the variation of P-wave velocity c_p. The maximum value was $B = 0.61$, while for plane-strain compression conducted at $P' = 5\,\text{MPa}$, the maximum was $B = 0.58$. This difference in the results is not due to experimental error but to anisotropy of the material and loading. As explained in §3b, pure hydrostatic loading cannot be applied in plane-strain testing because, by definition, the intermediate principal stress σ_y limits deformation and is not controlled. Thus, when $\Delta\sigma_1 = \Delta\sigma_3$ is applied, some deviatoric load is still present and slight anisotropic material behaviour affects the results [40]. The time scale of the saturation process depends on the geometry of the specimens and applied pressure gradients. The prismatic specimen of Berea sandstone was fully saturated within 1 day with application of $p > 4\,\text{MPa}$ ($P' = 5\,\text{MPa}$). However, when small back pressure increments (0.1 MPa) were applied for 10 days, the rock was fully saturated at $p = 1.3\,\text{MPa}$ ($P' = 1\,\text{MPa}$).

The alternative way to check saturation of a laboratory specimen is based on the observation that P-waves propagate in saturated geomaterials with a velocity that is strongly affected by water filling the voids [41]. Strachan [42] suggested the following criterion for ensuring full saturation: P-wave velocity in the saturated material becomes constant with increasing back pressure at constant Terzaghi effective mean stress. Two sensors were attached to the opposite sides of a prismatic specimen and P-wave velocity was measured during the saturation process

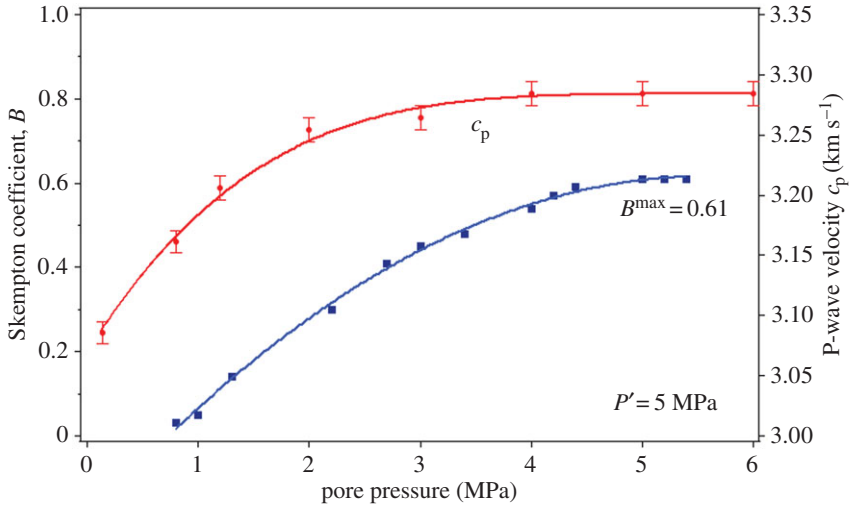

Figure 3. Change in the Skempton coefficient B and P-wave velocity with saturation at $P' = 5$ MPa. (Online version in colour.)

at $P' = 5$ MPa (figure 3). It can be seen that the velocity is increasing with the back pressure and becomes constant when p exceeds 4 MPa, which supports the proposed B-check method in achieving full saturation.

For unjacketed hydrostatic compression, the specimens were subjected to a high cell pressure (60 MPa), which was kept for a few hours to provide full saturation. Mercury intrusion porosimetry (MIP) tests on the Berea sandstone indicated that the rock was fully saturated with mercury (a non-wetting fluid) at pressures above 26 MPa, meaning that the minimum pore throat diameter is 0.027 µm. It can be expected that in the case of oil injection (wetting fluid for air-filled sandstone), full saturation can be reached at pore pressures not higher than 26 MPa and the unjacketed response (§4a) shows that this technique guaranteed satisfactory results.

4. Results and discussion

(a) Poroelastic parameters

Three prismatic 53 × 35 × 35 mm specimens were hydrostatically loaded and unloaded under jacketed and then unjacketed conditions. Linear strain measured in the direction perpendicular to bedding is 5–8% smaller than linear strain along the beds, which confirms a slight material anisotropy. Bulk moduli calculated from jacketed hydrostatic compression tests (in unloading) are found to be increasing with pressure: $K = 5$ GPa for $P = 2$ MPa, $K = 7$ GPa at $P = 5$ MPa and $K = 13$ GPa (and constant) when mean stress exceeded 30 MPa (figure 4). If the line corresponding to the constant slope of the dry compression curve is continued to intersect with the x-axis, the porosity of unstressed rock related only to the cracks that can be closed [43] is determined to be 0.003. The unjacketed bulk modulus is measured to be constant for pressures from 1 to 60 MPa: $K_s' = 29.4$–30.9 GPa. A fused quartz specimen was tested and its volumetric strain response is linear up to $P = 60$ MPa, with $K_{quartz} = 37.0$ GPa (figure 4).

Prismatic and cylindrical specimens of Berea sandstone were cut and then precisely ground from the same block in the same direction, such that the axial load was applied perpendicular to the bedding planes. The range of values for poroelastic parameters measured in eight plane-strain and two axisymmetric compression tests at $P' = 5.0$ MPa are presented in table 1. Reported plane-strain K and K_u values are obtained from calculation of total volume strain (including ε_2) caused by the increase in total mean stress. All reported undrained parameters are corrected for the compressibility of the drainage system (equations (3.7)–(3.10)), α in the calculated column is

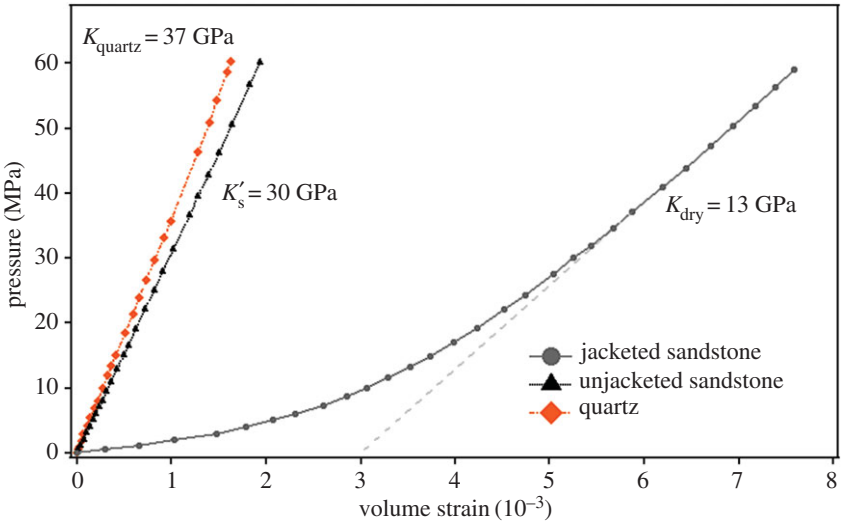

Figure 4. Results of jacketed and unjacketed hydrostatic compression tests on Berea sandstone and quartz. (Online version in colour.)

Table 1. Poroelastic parameters measured at $P' = 5$ MPa in plane-strain compression (PS) and axisymmetric (triaxial) compression (TC).

	measured								calculated		
test type	K (GPa)	K_u (GPa)	K'_s (GPa)	B	E (GPa)	E_u (GPa)	ν	ν_u	α	G (GPa)	M (GPa)
PS	9.4–10.0	14.6–16.3	—	0.58	10.8–11.3	13.7–15.1	0.30–0.32	0.35–0.36	—	4.1–4.3	—
TC	9.8–10.1	17.8–18.2	29.1–29.4	0.61	10.0–10.7	14.9–15.7	0.32–0.33	0.36–0.37	0.65–0.67	3.8–4.1	17.2–19.9

obtained from measured K and K'_s values (equation (2.12)), G values come from measured drained E and ν and M is calculated from K, K_u and α. An estimate of the Biot coefficient α was also attempted by measuring the change in pore volume from the fluid expelled from the specimen (equation (3.5)). The accuracy of the fluid volume measurements at pore pressures above 2 MPa is ± 0.02 ml, which is of the same order as measured drained water volumes due to application of $\Delta P = 5$ MPa in plane-strain and axisymmetric compression tests. Experiments at lower pressures ($P = 2.0$–2.5 MPa and $p = 1.5$ MPa) provide $\alpha = 0.86$.

Additionally, the evolution of drained and undrained bulk moduli K and K_u, Skempton B coefficient and Biot α coefficient (calculated from equation (2.12) for $K'_s = 30$ GPa) with Terzaghi effective pressure P' was studied in hydrostatic triaxial (axisymmetric) compression unloading tests performed on fully saturated specimens for $p = 4$–5 MPa. The obtained parameters are reported in table 2 and figure 5*a*,*b*, along with the experimental errors. Changing the loading rate two orders of magnitude (from $10^{-6}\,s^{-1}$ to $10^{-4}\,s^{-1}$) did not influence the drained (K) or undrained (B and K_u) properties. In terms of load history, the parameters measured in the first unloading cycle are approximately the same as those measured in the consecutive loading–unloading cycles.

The reported values of the unjacketed bulk modulus $K'_s = 29.1$–30.9 GPa are smaller than the measured bulk modulus of quartz $K_{quartz} = 37.0$ GPa, where it is often assumed $K_s = K'_s = K''_s$ for sandstones [4,33]. To investigate the observed difference, the microstructure was viewed in thin sections of the sandstone vacuum-impregnated with epoxy stained dye, both black and fluorescent. The analysis showed that some pores were not filled by the epoxy and hence contributed to the non-connected porosity. Precise measurements [44] of solid ($\rho = 2740\,kg\,m^{-3}$) and bulk density ($\rho = 2060\,kg\,m^{-3}$) of the rock revealed that the total porosity of the Berea

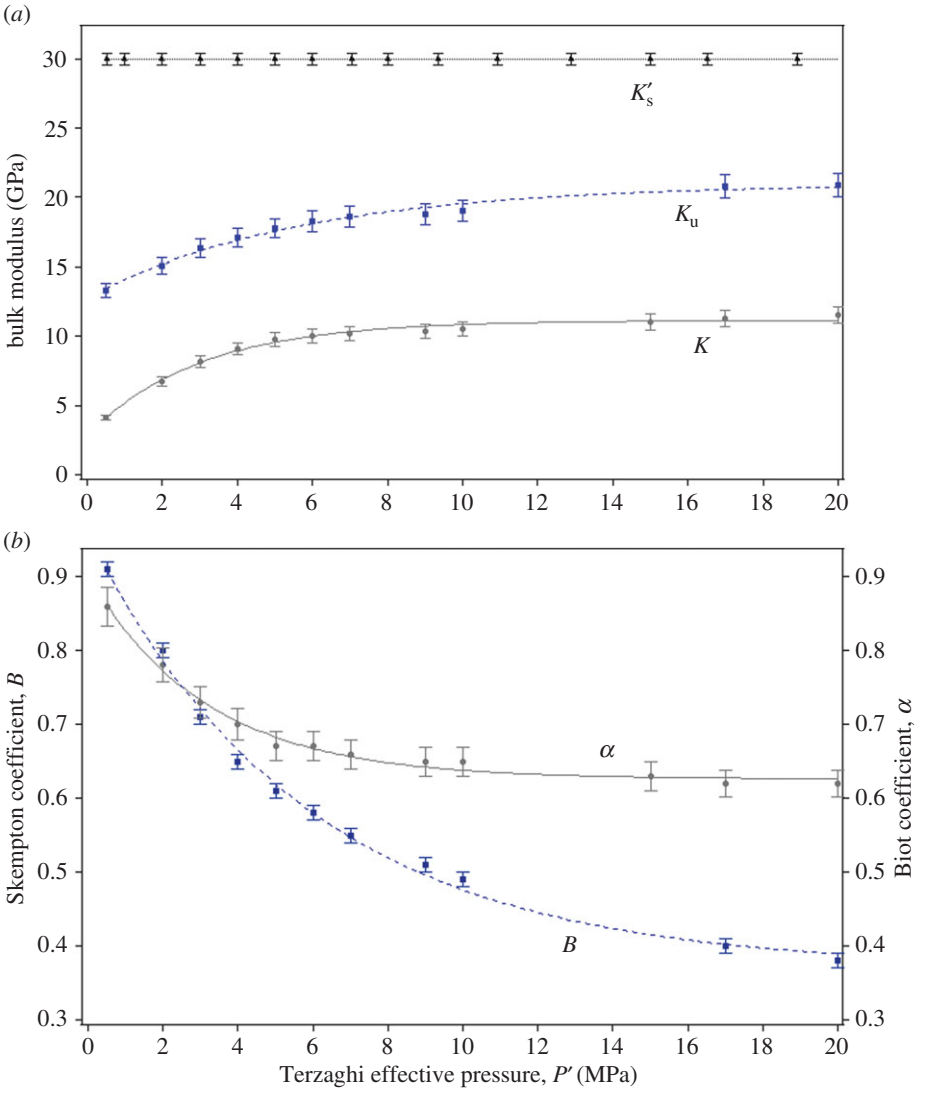

Figure 5. Evolution of poroelastic parameters with Terzaghi effective pressure: (*a*) bulk moduli, drained (K), undrained (K_u) and unjacketed (K'_s); (*b*) Skempton and Biot coefficients B and α. (Online version in colour.)

sandstone is equal to 0.25, which is larger than the interconnected porosity $\phi_o = 0.23$ measured consistently by vacuum saturation and MIP methods. The presence of non-connected pore space causes $K'_s < K_{quartz}$ and the assumption of $K_{quartz} = K'_s = K''_s$ may not be applicable for the tested rock.

Hydrostatic compression tests also show that the dry bulk modulus of Berea sandstone is a stress-dependent parameter at low mean stress and reaches its constant value $K = 13$ GPa only when $P > 35$ MPa. Because some other parameters, such as K_u, B and α, are dependent on dry rock properties (e.g. K), the material response can be treated as poroelastic and stress independent only at mean stresses greater than 35 MPa. However, the apparatus used for drained and undrained testing do not allow application of high (>24 MPa) hydrostatic pressure and hence most poroelastic parameters were observed to be stress dependent.

Figure 5 and table 2 illustrate the dependence of poroelastic parameters on the Terzaghi effective pressure $P' = P - p$, which is chosen as the simplest form of coupling mean stress P and pore pressure p. However, the question arises as to whether the magnitude of P' is the proper

Table 2. Poroelastic parameters K, K_u, B (measured in hydrostatic axisymmetric compression) and α (calculated for $K_s' = 30$ GPa) at various Terzaghi effective pressures $P' = P - p$ (measured at full saturation for $p = 4$–5 MPa).

$P' = P - p$ (MPa)	K (GPa)	K_u (GPa)	B	α
0.5	4.8	13.3	0.91	0.86
2	6.7	15.1	0.80	0.78
3	8.2	16.3	0.71	0.73
4	9.1	17.1	0.65	0.70
5	9.8	17.8	0.61	0.67
6	10.0	18.3	0.58	0.67
7	10.2	18.6	0.55	0.66
9	10.4	18.8	0.51	0.65
10	10.5	19.0	0.49	0.65
15	11.0	—	—	0.63
17	11.3	20.8	0.40	0.62
20	11.5	20.9	0.38	0.62

governing parameter for the measured poroelastic moduli, meaning that if P and p are varied but $P - p$ is preserved constant, the moduli should not change. The elastic change in total specimen volume was shown to be controlled (equations (2.8) and (2.19)) by the magnitude of $P - \alpha p$. Berryman [45] derived cumbersome effective stress expressions for porosity and permeability and demonstrated from the available experimental data that pore pressure is merely influencing changes in the volume of solid constituents. Todd & Simmons [46] suggested the following empirical form for expressing a small increment in any poroelastic parameter $N(P', p)$, e.g. bulk modulus, caused by a small change in pore pressure:

$$\mathrm{d}N = \left.\frac{\partial N}{\partial P'}\right|_{\mathrm{d}p=0} (\mathrm{d}P - n\mathrm{d}p), \tag{4.1}$$

where n is

$$n = 1 - \left.\frac{\partial N}{\partial p}\right|_{\mathrm{d}P'=0} \Big/ \left.\frac{\partial N}{\partial P'}\right|_{\mathrm{d}p=0}. \tag{4.2}$$

Following this approach, it can be shown from our data that the stress dependence of the Skempton coefficient B can be described through the Terzaghi effective pressure P', because changes in pore pressure at full saturation do not produce changes in B if $\mathrm{d}P' = 0$. The same is true for the drained bulk modulus K, but making a conclusive statement on stress dependence of the undrained bulk modulus K_u and the Biot coefficient α requires further testing.

From the results reported in tables 1 and 2, it can be seen that inequalities $0 \le K \le K_u \le K_s'$ and $0 \le \nu \le \nu_u \le 0.5$ are preserved. Results of the drained compression tests indicate approximately the same value for Poisson's ratio $\nu = 0.30$–0.32 but a lower value of Young's modulus $E = 10$–11 GPa than those obtained in dry uniaxial compression tests. Also, dry bulk modulus measured at $P = 5$ MPa in the hydrostatic jacketed compression is smaller than the one calculated from drained plane-strain and triaxial compression data: $K = 9.4$–10.1 GPa. These discrepancies between dry and drained parameters might be related to the different type of loading applied in those tests and its effect on closing cracks in rock. Indeed, values of K measured at $P' = 17$ and 20 MPa are close to values of dry bulk modulus measured at corresponding pressures in hydrostatic compression. Another explanation could be a different behaviour of the grain-to-grain contacts in the case of a fully dry rock compared with a water- or oil-saturated system [47].

The unjacketed pore volume bulk modulus K_s'' was measured over a range of $P = 1.5$–2.5 MPa and pore pressure $p = 1$–2 MPa and $K_s'' = 12 \pm 4$ GPa, which is significantly smaller than K_s', but still satisfies the theoretical lower limit: $K_s'' > \phi K_s'$ [20,30]. Modern syringe pumps allow accurate measurements of total and incremental volumes (approx. 0.1 µl), meaning that V_f and V_m from equation (3.6) can be measured precisely. The main error in K_s'' measurements is associated with the proper evaluation of dead volume V_L and the stiffness of the pore pressure measuring system C_{L+M}, which were calculated from calibration tests with a hollow-cylinder polyvinyl chloride specimen ($K = 3.8$ GPa and $K_s' = K_s'' = 6.7$ GPa). In our tests, the accuracy of V_L measurements is 0.5 ml and this causes the reported large range of K_s'' values. Note that if the unjacketed pore volume bulk modulus is calculated from stress-dependent parameters K, α and B (equation (2.14)), then K_s'' is a stress-dependent parameter itself.

Finally, the shear modulus $G = 4.1$–4.3 GPa calculated from the drained deviatoric loading was found to be smaller than the undrained one: $G = 4.9$–5.9 GPa. This violates the requirement of isotropic poroelasticity, as these two parameters should be the same. Berryman [48] showed that such a discrepancy in shear moduli can be explained by anisotropy of the tested material. The reported poroelastic parameters are in some agreement with the experimental observation of Hart & Wang [23], who performed drained and undrained conventional triaxial tests on Berea sandstone. They measured $K = 3.4$–5.9 GPa, $K_u = 11.1$–14.3 GPa, $\nu_u = 0.32$–0.37 and $B = 0.61$–0.75 for the Terzaghi effective pressure of 3–10 MPa; using these data, they found $K_s' = 27$–34 GPa.

(b) Inelastic response

Five drained and five undrained plane-strain compression experiments were conducted with increasing axial stress σ_1 (axial strain rate $= 10^{-6}\,\mathrm{s}^{-1}$) and the cell pressure σ_3 constant. We consider here a pair of drained and undrained tests that were performed with the same initial value of $P' = 5$ MPa (figure 6). The drained test started with $P = 8$ MPa; $\sigma_3 = 8$ MPa and $p = 3$ MPa were preserved throughout the test. During the undrained test, $\sigma_3 = 7$ MPa was kept constant; initial $P = 7$ MPa and pore pressure p evolved from 2 MPa to 4.5 MPa during elastic compaction and then decreased to 1.4 MPa at failure due to dilatancy.

The mechanical response is shown in figure 6*a*, where the peak shear stress $t_p = 44.4$ MPa for the drained test and $t_p = 48.1$ MPa for undrained. The increase in shear strength cannot be attributed entirely to dilatant hardening—captured by the first term in equation (2.32)—as Terzaghi mean stress was also changing and the second term in equation (2.32) contributes. At failure, in drained compression $P' = 46.2$ MPa ($p = 3$ MPa) and in undrained compression $P' = 48.4$ MPa ($p = 1.4$ MPa). The behaviour at constant mean stress ($\mathrm{d}P = 0$) is considered in [49].

The total volume strain response (figure 6*b*) indicates that the specimen tested under undrained conditions compacted more than the drained specimen during the initial stage of loading. It is related to the fact that the onset of inelasticity is reached at a larger value of total shear strain and a larger effective mean stress in the undrained test ($\gamma = 5.0 \times 10^{-3}$ and $P' = 24.2$ MPa) than in the drained one ($\gamma = 3.1 \times 10^{-3}$ and $P' = 17.3$ MPa). In both cases, the rock dilated by a smaller amount before failure than it compacted at the beginning of loading.

The plane-strain apparatus and the elastic–plastic decomposition of principal strains (ε_1, ε_3) provide increments of plastic volume strain $\Delta\varepsilon^p$ and plastic shear strain $\Delta\gamma^p$:

$$\Delta\varepsilon^p = \Delta\varepsilon_1^p + \Delta\varepsilon_3^p = (\Delta\varepsilon_1^{meas} - \Delta\varepsilon_1^e) + (\Delta\varepsilon_3^{meas} - \Delta\varepsilon_3^e) \tag{4.3}$$

and

$$\Delta\gamma^p = \Delta\varepsilon_1^p - \Delta\varepsilon_3^p = (\Delta\varepsilon_1^{meas} - \Delta\varepsilon_1^e) - (\Delta\varepsilon_3^{meas} - \Delta\varepsilon_3^e). \tag{4.4}$$

Dilatancy factor β is calculated from equation (2.26) assuming plane-strain compression. In the drained test, β is found to be changing at the beginning of plastic deformation and then becoming approximately constant and equal to 0.45; β is calculated to reach larger values in the undrained test, increasing to 0.59 and then decreasing to 0.52 at failure (figure 7). This observation is consistent with the two other pairs of drained and undrained tests performed at approximately

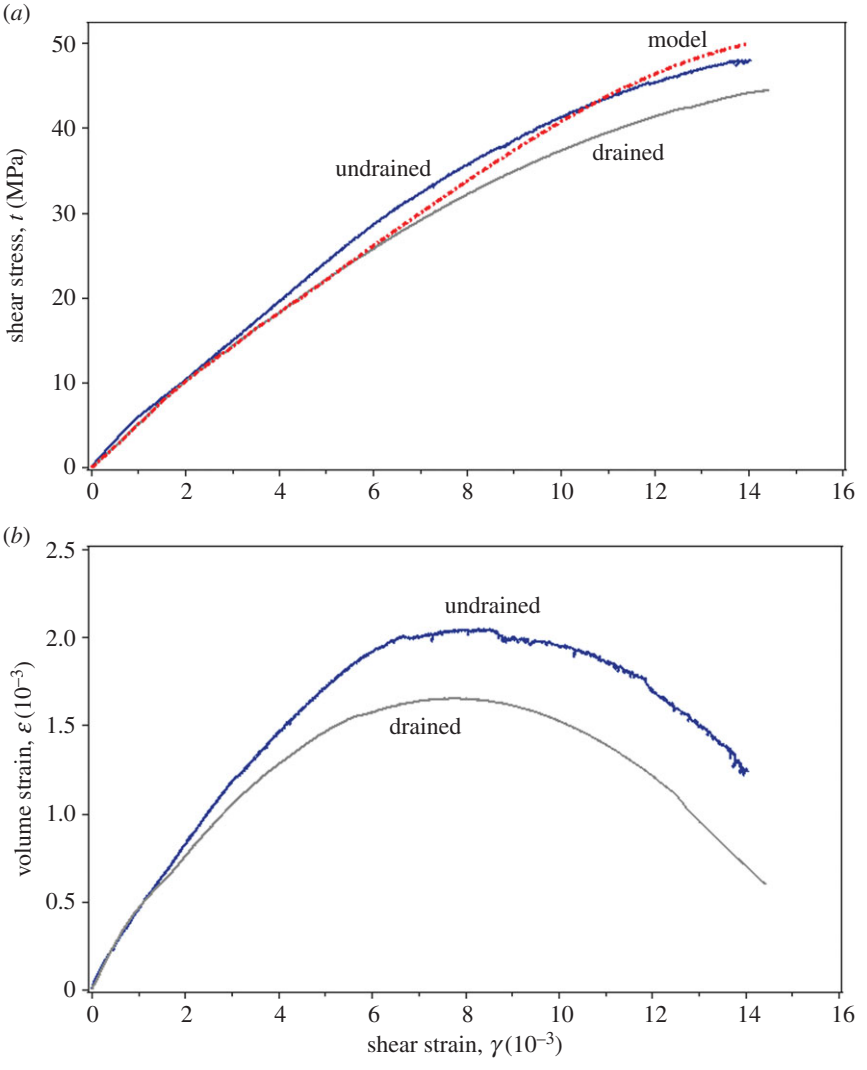

Figure 6. Drained and undrained plane-strain compression experiments with initial $P' = 5$ MPa. (*a*) Shear stress–shear strain response and model prediction; (*b*) total volume–shear strain response. (Online version in colour.)

the same P'. Possibly, there is some effect from pore pressure p, which was larger at the onset of inelasticity and at failure in the undrained tests. However, Sulem & Ouffrokh [50] found no difference in drained and undrained dilatancy factors measured at the same mean stress for Fontainebleau sandstone.

The friction coefficient μ is calculated assuming a linear yield function [51]:

$$\mu = \frac{\tau}{P' + V_o}, \tag{4.5}$$

where V_o is the uniform triaxial tensile strength and $V_o = 7.5$ MPa for Berea sandstone [52]. The friction coefficient μ is found to be increasing from 0.62 at onset of inelasticity to 0.78 at failure in the drained test and from 0.73 to 0.85 in the undrained test (figure 7). The constant values that dilatancy and friction attain in the drained test are used for model prediction: $\beta = 0.45$ and $\mu = 0.78$.

The change in interconnected porosity of the tested sandstone was smaller than 0.5% in all the tests, which is within the accuracy of the initial porosity measurements. Hence $\phi = \phi_o$ can be

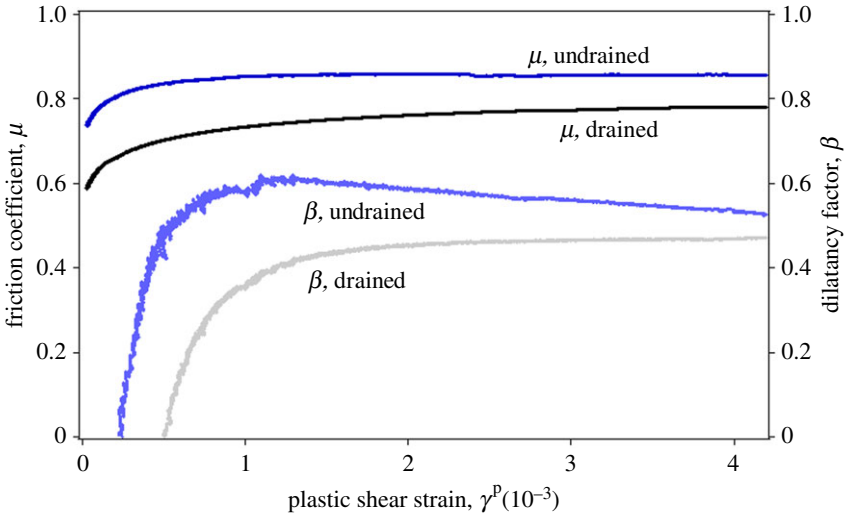

Figure 7. Friction coefficients μ and dilatancy factors β for drained and undrained compression experiments with initial $P' = 5$ MPa. (Online version in colour.)

assumed in (2.31) and according to equation (2.14) $K_{\text{eff}} = BK/\alpha$ and can be estimated for different Terzaghi effective mean stress values using the evolution of poroelastic parameters with stress from table 2. The inelastic hardening modulus H is determined from (2.25) for the drained test:

$$H = \frac{\Delta\tau - \mu\Delta P}{\Delta\gamma - \Delta\tau/G}. \tag{4.6}$$

To describe the corresponding undrained response, increments of shear stress are calculated from equation (2.32) by substituting the obtained values of μ, β, G, $K_{\text{eff}}(P')$ and H. The results of the drained and undrained tests, along with the model prediction, are presented in figure 6*a*.

The dilatant hardening behaviour is predicted for the undrained test approaching the maximum shear stress values based on the material parameters from the drained test. The response given by the model is softer than the experimental undrained response at the early stages of inelastic response. It is related to the larger value that the dilatancy factor takes at the beginning of undrained shearing compared with the drained one (figure 7). Additionally, the effect of intermediate principal stress, hidden in the dP term, and poroelastic anisotropy of the material [40] contribute to the discrepancy between predicted and the observed undrained deformation. Drained and undrained tests, where the mean stress can be preserved constant, provide the opportunity to directly observe dilatant response [49].

5. Conclusion

The behaviour of fluid-saturated rock was studied in the framework of Biot poroelasticity. A series of hydrostatic, plane-strain and conventional triaxial compression tests were performed on water-saturated Berea sandstone. Skempton B and Biot α coefficients, drained and undrained bulk moduli, and inelastic response (dilatancy) were measured. Drained and undrained poroelastic parameters varied with mean stresses below 35 MPa and the response of the material under undrained conditions was stiffer than the drained one. The unjacketed bulk modulus K_s' was directly measured and found to be constant at different mean stresses and $K_s' = 30$ GPa, 20% lower than the bulk modulus of quartz, usually assumed for this type of rock. This result is explained by the presence of non-connected pore space in the sandstone, which also causes the unjacketed pore bulk modulus K_s'' to be different than K_s'.

The results of drained and undrained plane-strain compression experiments with constant minimum principal stress were discussed in the framework of an elasto-plastic, hardening model. The parameters that govern the inelastic deformation of fluid-saturated rock, i.e. dilatancy factor β, friction coefficient μ, inelastic hardening modulus H, poroelastic coefficient K_{eff} and shear modulus G, were calculated from the drained response, and the model provided a first-order approximation of the undrained inelastic deformation.

Data accessibility. The data are available through the University of Minnesota Conservancy by contacting the corresponding author.

Authors' contributions. Both authors contributed to the work presented in this paper, designed and performed the experiments, discussed the issues, analysed the data, commented on the manuscript at all stages and gave final approval for publication.

Competing interests. The authors declare that they have no competing interests.

Funding. Partial support for this study was provided by DOE grant no. DE-FE0002020 funded through the American Recovery and Reinvestment Act.

Acknowledgements. Mr J. Meyer assisted with the development of the experimental apparatus. Profs E. Detournay and A. Drescher from the University of Minnesota provided helpful discussion.

References

1. Rice JR, Rudnicki JR. 1979 Earthquake precursory effects due to pore fluid stabilization of a weakening fault zone. *J. Geophys. Res.* **84**, 2177–2194. (doi:10.1029/JB084iB05p02177)
2. Roeloffs E. 1996 Poroelastic techniques in the study of earthquake-related hydrologic phenomena. *Adv. Geophys.* **37**, 135–195. (doi:10.1016/S0065-2687(08)60270-8)
3. Haimson BC, Fairhurst C. 1969 Hydraulic fracturing in porous-permeable materials. *J. Pet. Technol.* **21**, 811–817. (doi:10.2118/2354-PA)
4. Rice JR, Cleary MP. 1976 Some basic stress diffusion solutions for fluid-saturated elastic porous media with compressible constituents. *Rev. Geophys. Space Phys.* **14**, 227–241. (doi:10.1029/RG014i002p00227)
5. Detournay E, Cheng AHD. 1993 Fundamentals of poroelasticity. In *Comprehensive rock engineering*, vol. II (ed. C Fairhurst), pp. 113–171. Oxford, UK: Pergamon Press.
6. van der Kamp G, Gale JE. 1983 Theory of earth tide and barometric effects in porous formations with compressible grains. *Water Resour. Res.* **19**, 538–544. (doi:10.1029/WR019i002p00538)
7. Wang HF. 2000 *Theory of linear poroelasticity with applications to geomechanics and hydrogeology*. Princeton, NJ: Princeton University Press.
8. Han D, Batzle ML. 2004 Gassmann's equation and fluid-saturation effects on seismic velocities. *Geophysics* **69**, 398–405. (doi:10.1190/1.1707059)
9. Mavko G, Mukerji T, Dvorkin J. 1998 *The rock physics handbook*. Cambridge, UK: Cambridge University Press.
10. Rutqvist J. 2012 The geomechanics of CO_2 storage in deep sedimentary formations. *Geotech. Geol. Eng.* **30**, 525–551. (doi:10.1007/s10706-011-9491-0)
11. Brace WF, Martin RJ. 1968 A test of the law of effective stress for crystalline rocks of low porosity. *Int. J. Rock Mech. Mining Sci.* **5**, 415–436. (doi:10.1016/0148-9062(68)90045-4)
12. Rice JR. 1975 On the stability of dilatant hardening for saturated rock masses. *J. Geophys. Res.* **80**, 1531–1536. (doi:10.1029/JB080i011p01531)
13. Biot MA. 1935 Le problème de la consolidation des matières argileuses sous une charge. *Ann. Soc. Sci. Bruxelles* **B55**, 110–113.
14. Biot MA. 1941 General theory of three-dimensional consolidation. *J. Appl. Phys.* **12**, 155–164. (doi:10.1063/1.1712886)
15. Terzaghi K. 1923 Die berechnung der durchlassigkeitsziffer des tones aus dem verlauf der hydrodynamischen spannungsercheinungen. *Sitzungsber. Akad. Wissen. Wien Math. Naturwiss. Kl. Abt. Iia.* **132**, 105–124.
16. Biot MA, Willis DG. 1957 The elastic coefficients of the theory of consolidation. *J. Appl. Mech. Trans. ASME* **79**, 594–601.
17. Gassman F. 1951 Über die elastizität poröser medien. *Vierteljahrsschriftder Naturforschenden Gessellschaft Zurich* **96**, 1–23.

18. Geertsma J. 1957 The effect of fluid pressure decline on volumetric changes of porous rocks. *Trans. AIME* **210**, 331–340.
19. Geertsma J. 1966 Problems of rock mechanics in petroleum production engineering. In *Proc. 1st Congress of International Society for Rock Mechanics, Lisbon, Portugal, 25 September–1 October 1966*, vol. 1, pp. 585–594.
20. Brown RJ, Korringa J. 1975 On the dependence of the elastic properties of a porous rock on the compressibility of the pore fluid. *Geophysics* **40**, 608–616. (doi:10.1190/1.1440551)
21. Skempton AW. 1954 The pore-pressure coefficients A and B. *Geotechnique* **4**, 143–147. (doi:10.1680/geot.1954.4.4.143)
22. Green DH, Wang HF. 1986 Fluid pressure response to undrained compression in saturated sedimentary rock. *Geophysics* **51**, 948–956. (doi:10.1190/1.1442152)
23. Hart DJ, Wang HF. 2010 Variation of unjacketed pore compressibility using Gassmann's equation and an overdetermined set of volumetric poroelastic measurements. *Geophysics* **75**, 9–18. (doi:10.1190/1.3277664)
24. Nur A, Byerlee JD. 1971 An exact effective stress law for elastic deformation of rock with fluids. *J. Geophys. Res.* **76**, 6414–6419. (doi:10.1029/JB076i026p06414)
25. Rudnicki JW. 1985 Effect of pore fluid diffusion on deformation and failure of rock. In *Mechanics of geomaterials* (ed. ZP Bažant), pp. 315–347. New York, NY: John Wiley & Sons.
26. Rice JR. 1977 Pore pressure effects in inelastic constitutive formulations for fissured rock masses. In *Advances in civil engineering through engineering mechanics*, pp. 360–363. New York, NY: ASCE.
27. Vardoulakis I, Goldscheider M. 1981 Biaxial apparatus for testing shear bands in soils. In *Proc. 10th Int. Conf. on Soil Mechanics and Foundation Engineering, Stockholm, Sweden, 15–19 June 1981*, pp. 819–824. Amsterdam, The Netherlands: A. A. Balkema.
28. Labuz JF, Dai S-T, Papamichos E. 1996 Plane-strain compression of rock-like materials. *Int. J. Rock Mech. Min. Sci.* **33**, 573–584. (doi:10.1016/0148-9062(96)00012-5)
29. Makhnenko R, Labuz J. 2014 Plane strain testing with passive restraint. *Rock Mech. Rock Eng.* **47**, 2021–2029. (doi:10.1007/s00603-013-0508-2)
30. Cheng AHD. 2016 *Poroelasticity*. Cham, Switzerland: Springer International Publishing.
31. Wissa AE. 1969 Pore pressure measurements in saturated stiff soils. *ASCE J. Soil Mech. Found. Div.* **95**, 1063–1073.
32. Bishop AW. 1976 Influence of system compressibility on observed pore pressure response to an undrained change in stress in saturated rock. *Géotechnique* **26**, 371–375. (doi:10.1680/geot.1976.26.2.371)
33. Mesri GK, Adachi K, Ullrich CR. 1976 Pore-pressure response in rock to undrained change in all-round stress. *Géotechnique* **26**, 317–330. (doi:10.1680/geot.1976.26.2.317)
34. Ghabezloo S, Sulem J. 2010 Effect of the volume of the drainage system on the measurement of undrained thermo-poro-elastic parameters. *Int. J. Rock Mech. Min. Sci.* **47**, 60–68. (doi:10.1016/j.ijrmms.2009.03.001)
35. Brown ET. 1981 *Rock characterization, testing and monitoring: ISRM suggested methods*. Oxford, UK: International Society for Rock Mechanics, Pergamon Press.
36. Lin Q, Labuz JF. 2013 Fracture of sandstone characterized by digital image correlation. *Int. J. Rock Mech. Min. Sci.* **60**, 235–245. (doi:10.1016/j.ijrmms.2012.12.043)
37. Makhnenko RY, Labuz JF. 2013 Saturation of porous rock and measurement of the B-coefficient. In *Proc. 47th US Rock Mechanics/Geomechanics Symp., San Francisco, CA, 23–26 June 2013*, paper no. 468, vol. 1, pp. 679–684. Alexandria, VA: American Rock Mechanics Association.
38. Lowe J, Johnson TC. 1960 Use of back pressure to increase degree of saturation of triaxial test specimen. In *Proc. ASCE Research Conf. on Shear Strength of Cohesive Soils, Boulder, CO, June 1960*, pp. 819–836.
39. Schuurman IE. 1966 The compressibility of an air/water mixture and a theoretical relation between the air and water pressures. *Geotechnique* **16**, 269–281. (doi:10.1680/geot.1966.16.4.269)
40. Makhnenko RY. 2013 Deformation of fluid-saturated porous rock. PhD dissertation, Department of Civil Engineering, University of Minnesota, Minneapolis, MN, USA.
41. Bardet JP, Sayed H. 1993 Velocity and attenuation of compressional waves in nearly saturated soils. *Soil Dyn. Earthquake Eng.* **12**, 391–401. (doi:10.1016/0267-7261(93)90002-9)

42. Strachan P. 1985 Alternative test method for ensuring full saturation in triaxial samples. *Geotech. Testing J.* **8**, 43–46. (doi:10.1520/GTJ10857J)
43. Walsh JB. 1965 The effect of cracks on compressibility of rock. *J. Geophys. Res.* **70**, 381–389. (doi:10.1029/JZ070i002p00381)
44. Peron H, Hueckel T, Laloui L. 2007 An improved volume measurement for determining soil water retention curves. *Geotech. Testing J.* **30**, 1–8. (doi:10.1520/GTJ100167)
45. Berryman JG. 1992 Effective stress for transport properties of inhomogeneous porous rock. *J. Geophys. Res.* **97**, 17 409–17 424. (doi:10.1029/92JB01593)
46. Todd T, Simmons G. 1972 Effect of pore pressure on the velocity of compressional waves in low-porosity rocks. *J. Geophys. Res.* **77**, 3731–3743. (doi:10.1029/JB077i020p03731)
47. Berryman JG. 2010 Poroelastic measurement schemes resulting in complete data sets for granular and other anisotropic porous media. *Int. J. Eng. Sci.* **48**, 446–459. (doi:10.1016/j.ijengsci.2009.11.005)
48. Berryman JG. 2005 Poroelastic fluid effects on shear for rocks with soft anisotropy. *Geophys. J. Int.* **161**, 881–890. (doi:10.1111/j.1365-246X.2005.02581.x)
49. Makhnenko RY, Labuz JF. 2015 Dilatant hardening of fluid-saturated sandstone. *J. Geophys. Res. Solid Earth* **120**, 909–922. (doi:10.1002/2014JB011287)
50. Sulem J, Ouffroukh H. 2006 Shear banding in drained and undrained triaxial tests on a saturated sandstone: porosity and permeability evolution. *Int. J. Rock Mech. Min. Sci.* **43**, 292–310. (doi:10.1016/j.ijrmms.2005.07.001)
51. Riedel JJ, Labuz JF. 2007 Propagation of a shear band in sandstone. *Int. J. Numer. Anal. Methods Geomech.* **31**, 1281–1299. (doi:10.1002/nag.592)
52. Makhnenko RY, Harvieux J, Labuz JF. 2015 Paul-Mohr-Coulomb failure surface of rock in the brittle regime. *Geophys. Res. Lett.* **42**, 6975–6981. (doi:10.1002/2015GL065457)